Ocean Modelling 177 (2022) 102092

Contents lists available at ScienceDirect

Ocean Modelling

journal homepage: www.elsevier.com/locate/ocemod

# Characterizing vertical upper ocean temperature structures in the European Arctic through unsupervised machine learning

Erin E. Thomas [a,*], Malte Müller [a,b]

[a] Norwegian Meteorological Institute, Postboks 43 Blindern, 0313 Oslo, Norway
[b] Department of Geosciences, University of Oslo, Oslo, Norway

ARTICLE INFO

Dataset link: https://doi.org/10.48670/moi-00001, https://doi.org/10.48670/moi-00036

*Keywords:*
Self-organizing maps
Unsupervised neural network
Arctic ocean
Vertical temperature structures
Argo
CTD

ABSTRACT

In-situ observations of subsurface ocean temperatures are, in many regions, inconsistently distributed in time and space. These spatio-temporal inconsistencies in the observational network lead to difficulties in utilizing those observations effectively for ocean model evaluation or understanding larger-scale ocean characteristics. Model accuracy of subsurface ocean characteristics is especially important within regions that contain complex ocean structures. One such region is the European Arctic which not only contains several types of water masses with unique characteristics, but also wintertime sea ice coverage and complex bathymetry. This study presents an unsupervised neural networking technique that can be used in combination with traditional ocean model evaluation techniques to provide additional information on the accuracy of modeled vertical ocean temperature profiles. Self-organizing maps is an unsupervised machine learning technique that we apply to approximately twenty thousand Argo and CTD temperature profiles from 2012 to 2020 in the European Arctic to categorize the observed vertical ocean temperature structures in the top 150 m. The observed ocean profile categories, or neurons, defined by the self-organizing map show strong spatial and temporal dependencies. We then use the neuron weights, or the learned temperature profile structure of each neuron, to validate the spatial and temporal variability of modeled vertical temperature structures. This analysis gives us new insights about the model's capabilities to reproduce specific vertical structures of the top-most ocean layer within different regions and seasons. Mapping modeled ocean temperature profiles onto the neuron-space of the observationally-defined self organized map highlights the potential of this method to advance our understanding of model deficiencies in that region.

## 1. Introduction

In coupled ocean–atmosphere model systems many challenges are connected to the accurate representation of the air-sea heat, momentum, and mass fluxes (Cronin et al., 2019; Giorgi, 2019). In order to advance simulations of the ocean–atmosphere heat exchange, accurately simulating the upper few hundred meters of the ocean water column is necessary due to its large impact on sea surface temperature variability and in turn the heat and moisture fluxes to the atmosphere (D'Asaro, 2014). Thus, not only sea surface temperature, but also ocean subsurface observations are critical to understand coupled ocean–atmosphere model characteristics.

The main observation source for upper ocean temperature is provided by autonomous floats of the Argo program and ship-based CTD measurements (Wong et al., 2020). The spatio-temporal patterns of those in-situ observations are, however, highly irregular in space and time. Thus, using observed profiles for model evaluation is difficult and further challenged by the issue of representativeness of a point observation versus a gridded model solution. Due to these inconsistencies, model verification studies often use climatological products, e.g. the World Ocean Atlas, or ocean reanalysis products. However, in order to preserve the fine-scale structure of upper ocean profiles, which is crucial for the short-term development of the sea surface temperature by vertical convective processes, it would be preferable to not smooth-out, for example a sharp mixed layer which is presented in the raw data, or other small spatial scale features such as eddies. This is especially important, and especially challenging, within regions that contain complex ocean structures and multiple types of water masses with unique temperature characteristics.

Utilizing an unsupervised categorization methodology in order to find systematic spatio-temporal patterns between upper ocean temperature profiles has the potential to make additional use of the large amount of existing Argo and CTD profiles (Jones et al., 2019; Sonnewald et al., 2021). The self-organizing map, hereafter referred to as SOM (Kohonen, 2001), is an unsupervised artificial neural network that is often used in meteorological and oceanographic applications (Liu

* Correspondence to: Fluid Dynamics and Solid Mechanics (T-3), Los Alamos National Laboratory, Los Alamos, NM, USA.
*E-mail addresses:* ethomas@lanl.gov (E.E. Thomas), maltem@met.no (M. Müller).

https://doi.org/10.1016/j.ocemod.2022.102092
Received 26 April 2022; Received in revised form 29 July 2022; Accepted 30 July 2022
Available online 4 August 2022

and Weisberg, 2011; Iskandar et al., 2008; Richardson et al., 2003; Liu et al., 2016) to simplify and map highly complex spatio-temporal data onto a simplified 2-dimensional space. In the present study, we apply SOM to a set of Argo and CTD profiles of the upper 150m for the region of the Nordic and Barents Seas and show how this method can be complimentary to more traditional ocean model evaluation techniques to provide additional information on the accuracy of modeled vertical ocean temperature profiles. This paper is organized as follows: Section 2 describes the data used. Section 3 describes the SOM methodology. Section 4 presents the results of the SOM analysis as well as the model evaluation while Section 5 contains a discussion.

## 2. Data

### 2.1. Observations

We use a combination of in-situ temperature observations (primarily Argo and CTD profiles) between 2012 and 2020 obtained through the Copernicus Marine Service Monitoring Service (Wong et al., 2020; Wehde et al., 2021). We interpolate each temperature profile within the European Arctic domain to vertical coordinates every 1m and only keep data in the top 150m of the water column. Profiles that either do not reach a depth of at least 150m or do not contain temperature data in the top 10m are ignored. The resulting total number of observed temperature profiles used in this study equals 24,742.

### 2.2. Ocean model

Ocean model simulation output of the TOPAZ4 model is used for comparison. The TOPAZ4 model is part of the Copernicus Marine Environmental Monitoring Service (CMEMS) — Arctic Marine Forecasting Center (ARC-MFC), which is a forecasting system producing daily 10-day ensemble forecasts (Sakov et al., 2012). The forecasting system is based on the hybrid coordinate ocean model (HYCOM) coupled to a sea ice model with the sea ice thermodynamics and the elastic–viscous–plastic rheology described in Hunke and Dukowicz (1997). The weekly data assimilation system used in TOPAZ4 is the Ensemble Kalman Filter. This is a multivariate assimilation technique that depends on the 100-member best estimate ensemble (Sakov et al., 2012). A suite of 10-member 10-day forecasts is performed daily, forced by the European Centre for Medium-Range Weather Forecasts (ECMWF) high resolution (HRES) weather forecast model (Bauer et al., 2013). TOPAZ uses the turbulent mixing sub-model from the Goddard Institute for Space Studies as described in Canuto et al. (2002).

The native horizontal grid of the TOPAZ model contains a resolution of approximately 12–16 km. However, output products are interpolated onto a grid with 12.5 km resolution. The native vertical resolution of the TOPAZ model uses 28 hybrid layers. The hybrid layers are defined so that the minimum thickness of the top most layer is 3 m, while the maximum thickness of other layers is 450 m. The output products, however, are only archived for 12 vertical z-layers. Sakov et al. (2012) and Melsom et al. (2012) provide additional details about the native TOPAZ model setup.

We use the daily ensemble-mean TOPAZ4 ocean temperature profiles for the year 2020. The TOPAZ model simulations are accessible through the Copernicus Marine Environmental Monitoring service on a z-level vertical grid with depths of 5, 30, 50, 100, 200, and 400m in the upper ocean. We interpolate all TOPAZ temperature profiles (at each spatial location for every day) to 1m depth intervals at spatial locations where temperature profiles are at least 200m (to ensure correct interpolation to a depth of 150m). Each interpolated TOPAZ profile is truncated at a depth of 150m.

## 3. Self-Organizing Map

Self-Organizing Mapping is an unsupervised artificial neural network that is used for pattern recognition, classification, and clustering analysis (Kohonen, 2001). It has been widely used in the context of meteorological and oceanographic observation and model analysis (Liu and Weisberg, 2011; Liu et al., 2016; Landschützer et al., 2013, 2014). Unsupervised machine learning algorithms, including SOM, are able to learn and adjust their own classifications based on the input data alone, without any external or user input. In order to learn without external input, unsupervised algorithms assume that shared patterns exist within the input data. This assumption is appropriate for our application since temperature profiles within a given region share many characteristics.

SOMs are defined as a 2-dimensional map comprised of neurons. Each neuron is defined with a neuron weight, which are trained using a competitive learning algorithm. This means as each piece of data (in our case, a 'piece of data' is a single observed vertical temperature profile) is input during the iterative training process, there is only one winning neuron, also referred to as the 'Best Matching Unit', hereafter referred to as the BMU, to which that piece of data is assigned. In other words, only one neuron within the SOM can be activated during each iteration of the training process. For each piece of input data, the structure of the activated neuron is adjusted to closer match the new data assigned to it. However, it is possible to allow each activated neuron to also influence the structure of the neighboring neurons. Neurons in a SOM are, therefore, more similar to their neighboring neurons than they are to neurons located farther away in the 2-D SOM-space. This competitive learning process and neighborhood influence leads to the neurons within the SOM organizing themselves.

### 3.1. Defining the SOM

Before training the SOM to the observational temperature data, the spatial structure of the 2-dimensional SOM-space must be defined. In most cases, the best results occur when the physical space of the observations is similar in shape to that of the SOM. Since our Arctic domain is approximately square, the best results occur from a SOM also containing a square shape.

Increasing the total number of neurons in the SOM generally results in a better fit (meaning each individual temperature profile better matches their assigned neurons), however, using too many neurons does not sufficiently reduce the data to provide useful information about the characteristics of the data. On the other hand, defining a SOM with very few neurons generally results in a poor fit between any given profile and its assigned neuron weight.

We use the SOM quantization error (Q-error) to determine the fit of a data set to the trained SOM weights. The Q-error is calculated as the mean euclidean distance between the data and neuron weights, where smaller Q-error values indicate stronger fit of the data to the neuron weight. The Euclidean distance (in units K) between any two temperature profiles (such as an observation and a neuron weight) is calculated as follows:

$$D = \sqrt{\sum_{i=0}^{dmax} (T_{i,A} - T_{i,B})^2}, \quad (1)$$

where $D$ is the Euclidean distance, $dmax$ is 150 m (the maximum depth of the profiles), and $T_{i,A}$ and $T_{i,B}$ are the temperatures of profiles $A$ and $B$, respectively, at a depth of $i$m.

Although the size of the SOM is ultimately selected by the user, a suite of sensitivity studies testing multiple SOM sizes, results shown in Fig. 1, helps determine an appropriate size. Fig. 1 shows the Q-error is relatively constant at large SOM sizes. In other words, small SOM sizes result in large errors due to inadequate separation between profile types, however, very large SOM sizes are not useful either as they do not strongly improve the Q-error nor sufficiently reduce the dimensionality of complex data. Fig. 1 shows a SOM with the size


**Fig. 1.** Self Organizing Map Quantization-Error (Q-error; in units K) plotted as a function of Self Organizing Map (SOM) Size. The Q-error is calculated as the Mean Euclidean distance between each observation and the neuron weight of their best matching unit (BMU) and measures how well the data fits the trained SOM. The size of the SOM chosen for use in this study is 6 neurons $x$ 6 neurons for a total of 36 neurons. The 6 × 6 SOM size provides a low Q error (meaning the raw data agrees well with the trained neuron weights) as well as provides a nice balance between simplifying the complexity of the original data while adequately separating different vertical temperature structures (important for classification).

of 6 × 6 neurons, for a total of 36 neurons, results in a low Q-error (meaning the raw data agrees well with the learned neuron weights). This size both simplifies the complexity of the original data while adequately separating unique vertical temperature structures which is important for classification and model evaluation. The Q-error of the 6 × 6 SOM trained to the observation temperature data is 5.75K (Fig. 1).

### 3.2. Training the SOM

The first step of training the SOM is initializing each neuron weight. We initialize the weights using a randomly selected observed temperature profile from the data set. The SOM is then 'trained' on the observed temperature profiles through an iterative process: one randomly selected temperature profile from the data set is input at a time and the SOM algorithm determines which neuron weight it best matches. The 'winning' neuron, or best matching unit (BMU), is determined by minimizing the euclidean distance between the observation and the neuron weight (see Eq. (1)). The structure of the BMU weight is then adjusted toward the structure of the new data assigned to it.

During the training of the SOM, we allow the winning neurons to weakly influence the structure of their neighbors. This results in the SOM organizing itself so that neurons will share similar characteristics to their neighbors. The neighborhood function of the SOM defines how the winning neurons influence their neighbors. We define the neighborhood function to be Gaussian in space with a sigma value of 1.25.

The training process also depends on a learning rate parameter and the total number of iterations. The 6 × 6 SOM in this study is trained using a learning rate of .7 and 20,000 iterations. Several sensitivity tests (not shown) determined the structures of the SOM neuron weights are not sensitive to adjustments in the learning rate or the number of iterations used assuming the number of iterations used to train the SOM is appropriate for the size of the input data set. We found that for our data set, containing approximately 24,000 temperature profiles, values between 10,000 iterations and 20,000 iterations in the training process had a negligible impact on the results.

As previously mentioned in Section 3.1, the Q-error, which estimates the fit of the data to the SOM weights, is strongly influenced by the SOM size used. However, the structures identified within a given SOM size are robust. In other words, re-training a 6 × 6 SOM on the observational temperature data consistently produces similar temperature structures although the location of any given structures within the 6 × 6 SOM-space changes. We have high confidence in the ability of the SOM temperature classifications due to the robustness of temperature structures that result.

## 4. Results

### 4.1. The study region: Nordic and Barents Seas

Our study region is a part of the European Arctic, including the Greenland Sea, Lofoten Basin and Barents Sea (Fig. 2). The Norwegian Meteorological Institute operates a convective-scale weather forecasting system (Müller et al., 2017) for this region with future endeavors to couple the atmospheric system to more realistic representations of ocean, sea-ice, and wave dynamics (Batrak and Müller, 2018, 2019; Thomas et al., 2021b). The upper ocean in this area is characterized by cold polar water masses from the North and the intrusion of warm Atlantic waters with its origin in the North Atlantic Current (NAC, Rossby, 1996). The boundary between the North Atlantic water mass and the Arctic water mass containing large gradients in temperature and salinity is called the Arctic Front (Swift and Aagaard, 1981; Raj et al., 2019). The inflow of relatively warm Atlantic water into the frontal region is through two NAC branches. First, the Norwegian Atlantic Slope Current (NwASC) following the Norwegian shelf edge as a barotropic slope current (Skagseth et al., 2004), and, second, the Norwegian Atlantic Front Current (NwAFC) flowing as a topography guided front current along the ridges dividing the Norwegian, Lofoten, and Greenland Basins (Mork and Skagseth, 2010). The NwASC further branches into a northward current towards the western side of the Svalbard Archipelago (West Spitsbergen Current, WSC) and into the Barents Sea though the Barents Sea Opening (Helland-Hansen and Nansen, 1909; Aagaard et al., 1985).

The spatial characteristics of the sea surface temperature (SST) in this area reflect the northward flowing warm Atlantic waters from the NwASC and NwAFC, areas of seasonal sea-ice, and the Arctic Front (Fig. 3). Again, the Arctic Front is characterized as the boundary between warm Atlantic water and Arctic water, which is most easily discussed through the behavior of the NwASC, NwAFC, and WSC (as seen in Fig. 2). The SST varies seasonally in all regions and a warm surface layer develops during summer. In particular, strong vertical temperature contrasts develop seasonally in basins which are not strongly influenced by the NwASC and NwAFC, for example, the Greenland Basin or Eastern Barents Sea (Raj et al., 2019).

### 4.2. Observed structures

In the following we highlight the potential of the SOM methods to reveal insights into the vertical structure of the upper O(100m) of the ocean which can be further used for evaluation purposes of gridded subsurface temperature products. We will first show the spatial and temporal patterns resulting from the SOM as applied to in-situ ocean temperature observations. We note that we only characterize upper

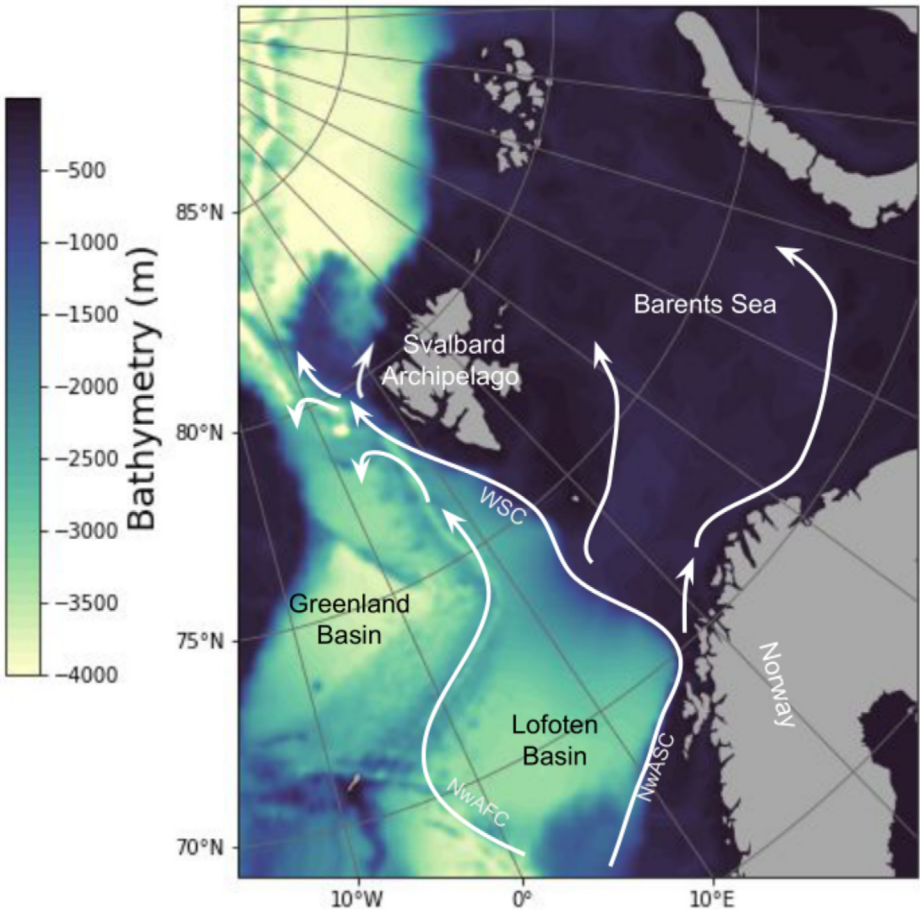


**Fig. 2.** The bathymetry of the study area in the European Arctic. It includes the Greenland and Barents Seas, as well as the Lofoten Basin. Ocean surface currents are indicated, i.e. the Northwest Atlantic Front Current (NwAFC), the Northwest Atlantic Slope Current (NwASC) and the West Spitsbergen Current (WSC).

ocean temperature profiles herein, thus the results and discussion below only characterize the vertical thermal stratification in the top 150m of the water column, and not the true stability of the water column as we do not include salinity in this analysis.

Fig. 4 shows the result of the SOM as applied to the observed temperature profiles. The SOM-learned profiles that define each neuron (numbered 1–36), also referred to as the neuron weights, are plotted with the thick black lines. The neuron weights represent the different types of temperature profiles observed in our region. The thin colored lines show each individual in-situ temperature profile sorted according to their best matching unit. Again, the BMU is determined by minimizing the euclidean distance between the observed profile and the neuron weight.

The structure of the 6 × 6 map of neurons can be summarized as follows (see also schematic in Fig. 5): the upper left (neuron 1), is characterized by a cold surface layer which deepens and becomes colder towards the right (moving from neuron 1 across the row towards neuron 6). Neuron 3 is unique in this series and contains a very distinct thin, cold surface layer in the top 20m. This top row represents temperature profiles that are non-thermally stratified. The neurons in the second and third rows (neurons 7 to 18) contain temperature profiles roughly described as well-mixed. Similar to row 1, these well mixed profiles become colder towards the right, decreasing from approximately 5 °C to 0 °C. The bottom three rows (neurons 19 to 36) contain profiles with stable thermal stratification (temperature decreases with increasing depth). These profiles typically become warmer as you move down through the rows, and increase in thermal stratification as you move downward and towards the right. Neuron 36 in the lower right corner of the SOM contains profiles that exhibit a relatively warm surface layer, a distinct thermocline at a depth of approximately 40m, and relatively cold water below the thermocline.

The boreal winter (DJF) and summer (JJA) distribution of observations sorted according to their BMU are shown in Supplemental Figures S2 and S3, respectively. Supplemental Figure S2 shows that wintertime observations are clustered in the neurons located in the top-left corner of the SOM-space, indicating wintertime profiles in this region are dominated by non thermally stratified and well-mixed temperature profiles. The summer observations contain larger spread in temperature characteristics and, thus, are distributed across a larger number of neurons than the winter profiles. Furthermore, the summer profiles contain thermally stratified profiles seen in the bottom left corner of the SOM; structures that are not observed during winter months.

The color scheme shown in Fig. 4 is specifically designed to be a two dimensional color gradient that visually represents similar characteristics shared between neighboring neurons. This color scheme which represents profile similarities is useful in spatial plots of the BMU. In the following discussion, we ask readers to refer to the neuron color scheme as defined in Fig. 4.

Fig. 6 shows the spatial distribution of observed temperature profiles for each season: DJF, MAM, JJA, SON. The color of each observation is based on the profile's BMU as defined in Fig. 4. Fig. 6 shows strong spatial and temporal patterns in the observed temperature profile characteristics captured by the SOM technique.

Temperature profiles north of 80N in every season are dominated by characteristics of very cold SST and upper ocean temperatures and contain increasing temperatures with depth. These characteristics occur primarily in the 'magenta' colored neurons (i.e. neurons 4–6; see Fig. 4).

During DJF and MAM, Fig. 6 shows the Greenland Basin (refer to Fig. 2 for the location) is dominated by cold temperature profiles as

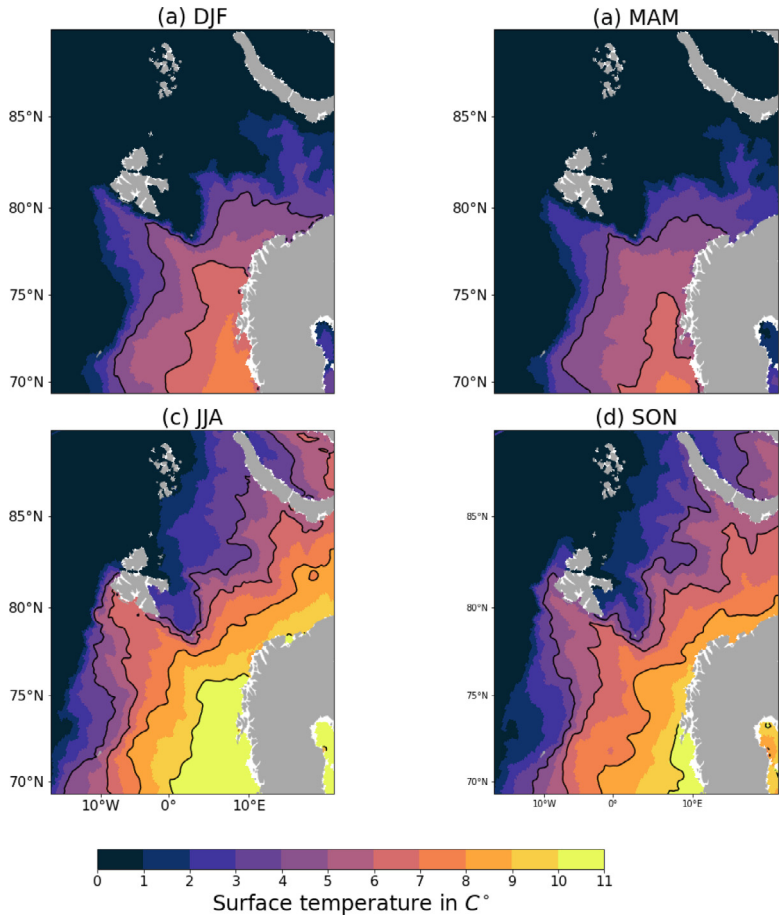


**Fig. 3.** Mean seasonal sea surface temperature (in degrees C) obtained from the TOPAZ4 forecasting system for 2020.

seen by the magenta and dark orange colored neurons (for example neurons 11, 12, 17, and 18). These temperature profiles are either thermally non-stratified or are cold and well-mixed to a depth of 150m. Specifically, these profiles are characterized by surface temperatures slightly above 0 °C while the waters below 50m are very close to 0 °C.

During JJA and SON, however, the Greenland Basin typically contains profiles with high thermal stratification (characterized by light-orange and yellow colored neurons; such as neurons 24, 30 or 36). The upper ocean in this region during the summer and fall contains relatively warm (with respect to the wintertime SST in the same region), shallow surface layers with depths of approximately 25m that contain temperatures of approximately 5 °C. The water temperature below the shallow surface layer is similar in structure and temperature as observed in the winter months characterized by cold temperatures of approximately 0 °C.

The Lofoten Basin (again, for the location refer to Fig. 2) is dominated by profiles containing much warmer ocean temperatures throughout the upper 150m during all seasons than observed in the Greenland Basin (Fig. 6). During DJF, the ocean temperature structure is characterized by well mixed profiles to a depth of 150m and contains temperatures approximately 5 °C. These profiles are characterized by, for example, neurons 7, 8, 13, and 14. During JJA, however, the Lofoten Basin contains temperature profiles with slight temperature stratification that the SOM categorizes as, for example, neurons 25, 26, and 31–33 (colored in royal-blue, and blue-gray). These stratified profiles contain warmer SST than the corresponding winter profiles. All the profiles in the Lofoten Basin, regardless of the season, share a key characteristic: relatively warm temperatures between 50–150m that remains above 5 °C all year (as opposed to the profiles in the Greenland Basin, which contain very cold waters close to 0 °C at depths below 50m).

The spatial and temporal patterns of observed ocean temperatures captured by the SOM shown in Fig. 6 correctly identify several key oceanographic characteristics of this region. The SOM captures the relatively warm Norwegian Atlantic current flowing into the region from the south, a portion of which continues as the West Spitsbergen Current flowing northwards on the western side of Svalbard. SOM clearly identifies a distinct separation between the upper ocean temperature characteristics seen in Greenland Basin versus the Lofoten Basin. Additionally, this technique captures the seasonal surface warming throughout the domain during the summer months as well as the persistent cold subsurface temperatures in the Greenland Basin.

The SOM technique described above is thus capable of identifying observed characteristics of upper ocean temperature structure in the European Arctic. Furthermore, SOM simplifies a potentially complex analysis by clustering vertical temperature profiles with similar characteristics together into neurons, essentially reducing the complexity of the original data. In the following section we show how the observationally-based neuron weights can be leveraged to provide useful information to analyze the spatial and temporal characteristics of gridded ocean products, for example from an ocean model.

### 4.3. Model evaluation

This section presents the results comparing the upper ocean temperature simulated by the TOPAZ model against observations. Rather than performing temporal or spatial averaging on the observations, which smooths out important fine-scale spatio-temporal characteristics, we leverage the observation-based SOM presented in the previous section. We note the purpose of this section is not to provide a robust evaluation of the TOPAZ model performance in the European Arctic, but rather,

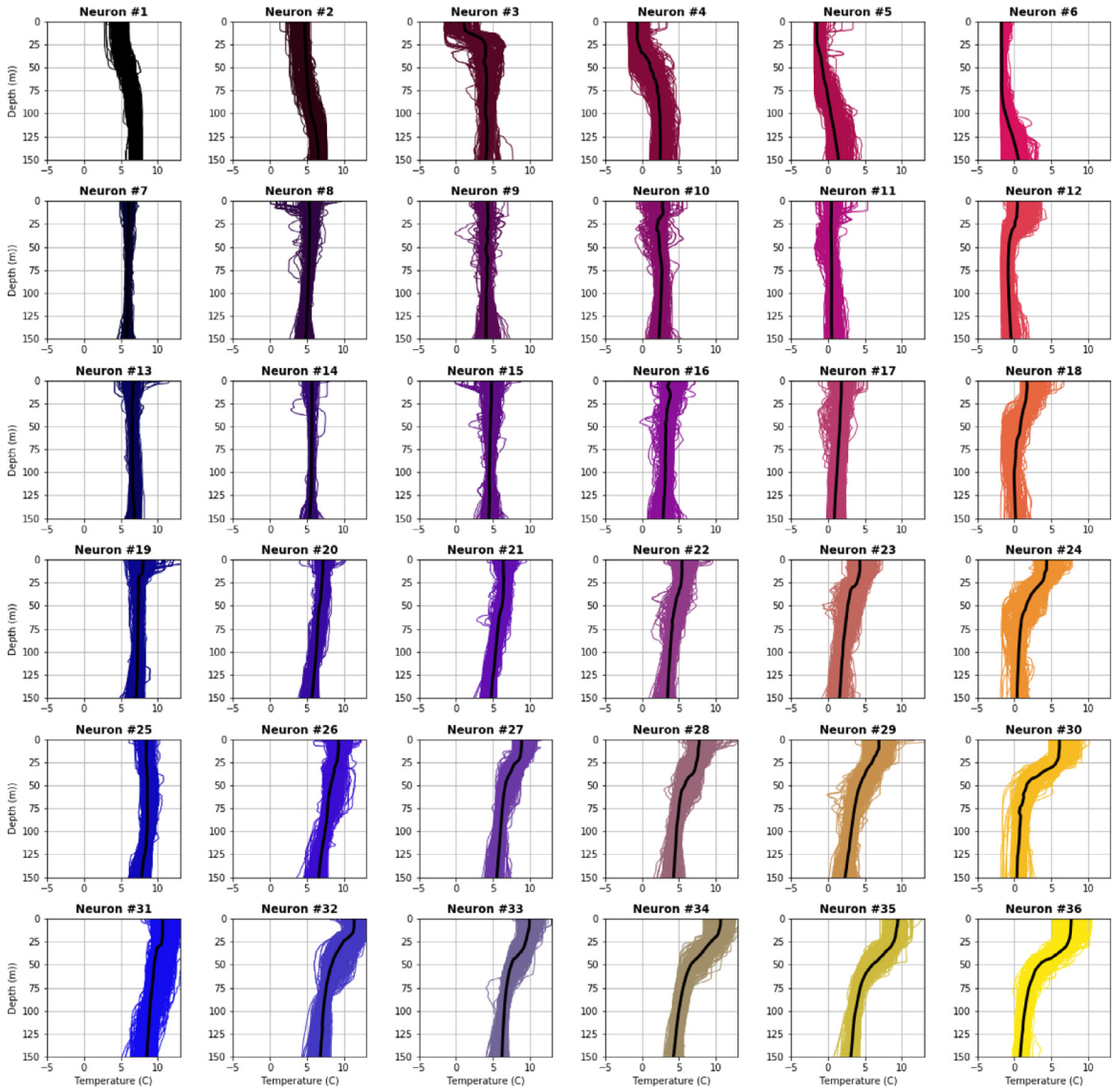


**Fig. 4.** Self Organizing Map neurons derived from Argo and CTD data (numbered 1–36). Neuron weights, or the temperature profile 'learned' by the SOM algorithm, are shown with the thick black lines, while individual Argo and CTD temperature profiles are shown with the thin, colored lines. The observations are plotted according to their best matching unit (BMU). See the text for details on how the BMU is determined.

we use the TOPAZ model to highlight additional insights of using SOM which are complimentary to more traditional model evaluation techniques.

While using the SOM neuron weights alone for evaluation may not be sufficient since they only show dominant profile characteristics smoothing out small scale features, Fig. 4, as well as Supplemental Figures S2 and S3, also show the raw observations, providing an estimate of the observed variability for any given neuron. We use these figures to analyze the TOPAZ model's ability to represent the fine scale patterns of variability seen in observations.

We first plot all DJF and JJA TOPAZ temperature profiles sorted according to the profile's BMU. Fig. 7 shows the DJF profiles while Fig. 8 shows the JJA profiles. The BMU of each TOPAZ profile is determined by the minimum Euclidean distance between the TOPAZ temperature profile and each SOM neuron weight. As in Fig. 4, the SOM neuron weights are shown in the thick, black lines in each Figure.

The most striking feature of the DJF and JJA TOPAZ profiles seen in Figs. 7 and 8 is the coarse vertical resolution of the model data. To quantify how well the TOPAZ model data fits the observed neuron weights we calculate the Q-error for each season for both observations and TOPAZ data. Table 1 shows the TOPAZ model contains larger Q-errors than the observations for every season. Unsurprisingly, this indicates the coarse vertical resolution TOPAZ data fits the neuron weights slightly worse than the observations do. The coarse vertical resolution and spatial smoothness of the model results in a loss of small-scale variability, thus, the TOPAZ data poorly captures the small-scale vertical features observed, such as the exact depth and temperature gradient of thermocline. Additionally, TOPAZ shows much greater variability in the SST for many neurons, especially neurons with thermal stratification. This large spread in SST can be seen, for example, in neurons 18, 24, 30 and 36.

To determine specific instances where the TOPAZ model may be under performing, we compare seasonal temperature profiles plotted in SOM-space. Supplemental Figures S2 and S3 are identical to Fig. 4, however, only contain DJF or JJA observations, respectively, plotted according to their BMU. Comparing Supplemental Figures S2 and S3 against Figs. 7 and 8 we can determine which observed temperature structures TOPAZ captures poorly.

In both DJF and JJA, TOPAZ generally reproduces the non-stratified and well-mixed profiles well. One exception to this is Neuron 3, where TOPAZ systematically fails to generate the thin, cold surface layer, seen in observations just north of the Svalbard archipelago. Another

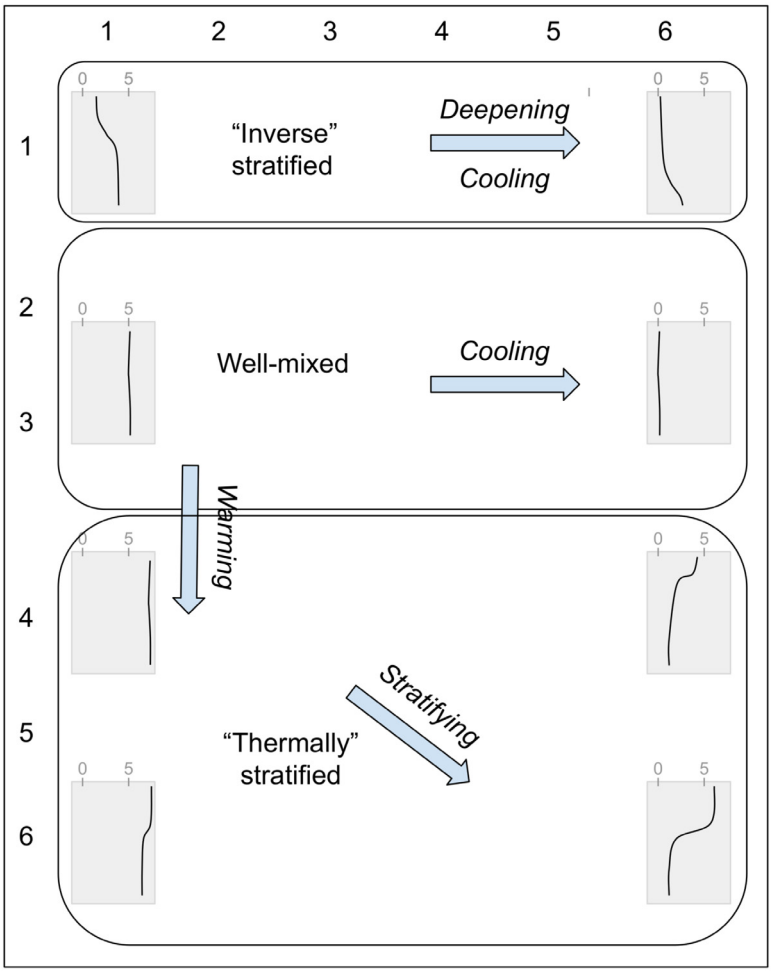


**Fig. 5.** Schematic showing the general characteristics of the neuron weights resulting from a 6 × 6 SOM trained on temperature observations in the European Arctic between 2012–2020. The term 'stratification' only refers to 'thermal' stratification, as we do not include salinity in this study to analyze the density stratification of the water column.

example of profile structures that are poorly represented in TOPAZ are the strongly stratified profiles observed in JJA (i.e. neurons 30 and 36). TOPAZ poorly represents the depth and gradient of the thermocline in these structures. Lastly, TOPAZ overestimates the SST in many of the thermally stratified neurons during JJA.

Next, we analyze how TOPAZ reproduces the observed spatial patterns of the profile types during each season. Similar to Fig. 6, Fig. 9 shows the spatial distribution of the neurons classified by TOPAZ for each season: DJF, MAM, JJA, and SON. Since we use ensemble-mean daily TOPAZ data in order to retain high frequency temporal variability, we determine TOPAZ model BMU for each day at every grid cell. Fig. 9 plots the BMU that occurs most often at every spatial point in each season (i.e. the colors represent the BMU 'mode' for the season).

Overall, TOPAZ captures the general spatial distribution of the profiles well. Similar to observations, TOPAZ contains very cold, well mixed profiles north of 80N. Additionally, it captures a general difference of profile characteristics between profiles in the Greenland Basin versus the Lofoten Basin. In TOPAZ, similar to observations, the Greenland Basin is generally dominated by non-thermally-stratified or cold, well-mixed temperature profiles in DJF and MAM, while more thermally stratified profile types occur during JJA and SON. As observed in the Lofoten Basin, TOPAZ also contains profiles that are well mixed or thermally-stratified. Lastly, TOPAZ captures the observed seasonal warming patterns observed which are particularly apparent in the Lofoten basin, where the top most ocean layer temperatures of the stratified profiles are warmer in JJA and SON than the temperatures captured in DJF and MAM.

Although TOPAZ captures some of the observed large scale temperature patterns, Fig. 9 also shows that TOPAZ fails to capture several key observed upper ocean temperature characteristics. For example, TOPAZ does not capture the distinct separation of temperature characteristics between in the Greenland basin and Lofoten basin profiles. Instead, TOPAZ contains a gentle gradient of profile characteristics between these two regions. Additionally, TOPAZ poorly captures the ocean structures observed in the West Spitsbergen Current along the west coast of Svalbard. Observations show the profiles in the West Spitsbergen Current are dominated by either relatively warm, well mixed profiles, or slightly stable profiles. TOPAZ, however, fails to capture these profile characteristics in every season, with the worst representation occurring during JJA, where the temperature structures in TOPAZ contain too much vertical temperature stratification.

## 5. Discussion

A thorough understanding of the observed upper ocean temperature patterns, especially in high latitude regions, is critical to accurately model the upper ocean. The accuracy of simulated upper ocean temperatures directly impacts the accuracy of modeled upper ocean mixing and surface heat fluxes. Thus, accurately simulating the upper ocean has large implications on the accuracy of coupled Arctic weather forecasts which are becoming increasingly critical as ship traffic in the Arctic due to industry and tourism is increasing and will continue to increase in the future (Hall and Saarinen, 2010; Smith and Stephenson, 2013; Stocker et al., 2020).

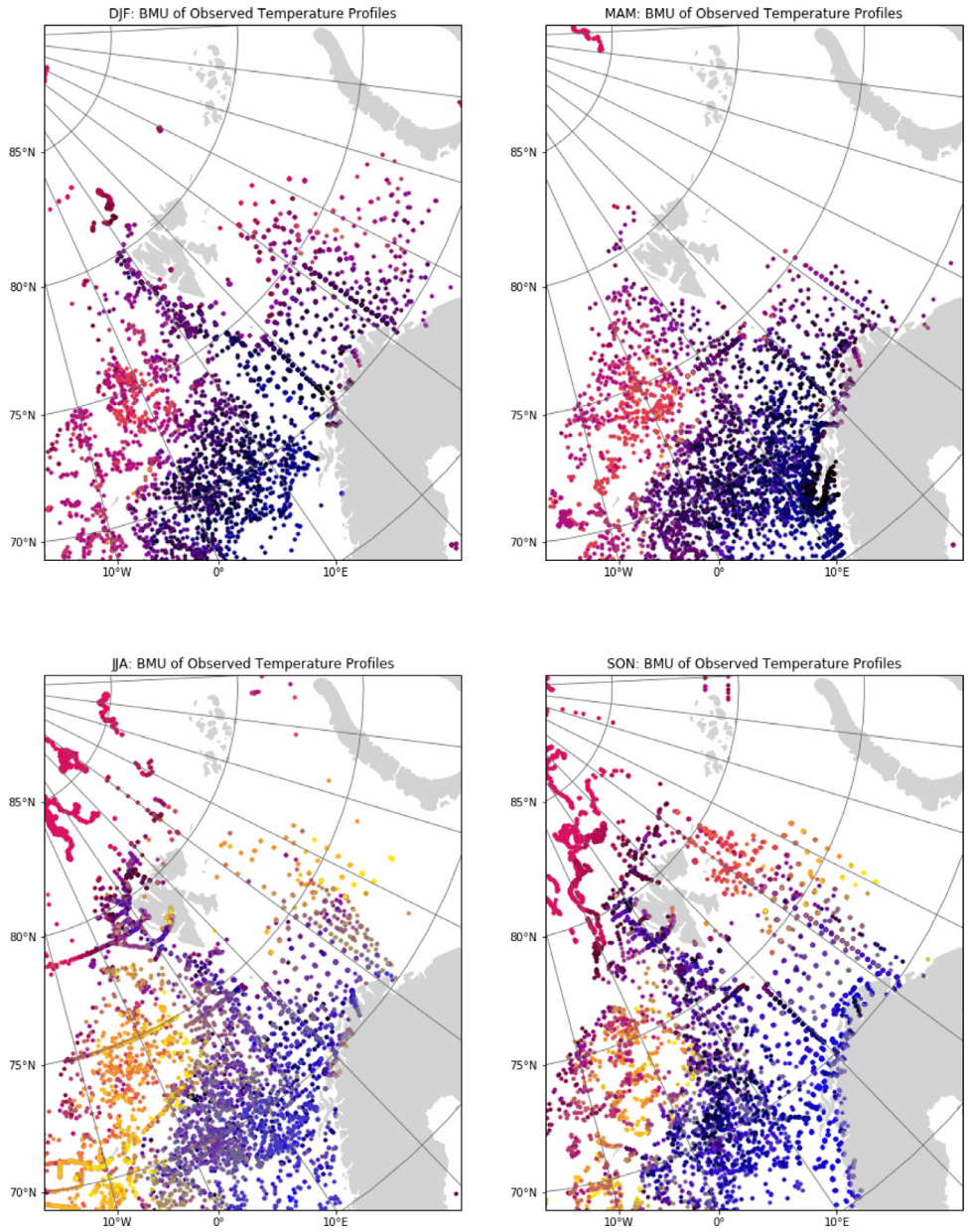


**Fig. 6.** Spatial distribution of all observed temperature profiles for each season: DJF, MAM, JJA, SON. The color of each observation represents the profile's best matching unit (BMU; numbered 1–36) as defined in Fig. 4. The BMU for each temperature profile is determined by the minimum Euclidean distance between the profile and each neuron weight.

Unfortunately, many ocean models and gridded ocean temperature products are either spatially smooth (in the horizontal), temporally smooth (such as climatology products), and/or have relatively coarse vertical resolution (such as the archived output from the TOPAZ ocean model). These characteristics increase the difficulty of regional model evaluation since gridded products typically under represent the observed spatial and temporal variability in the upper ocean.

In this study we use a machine learning technique called self-organizing maps, which has great potential in Earth and climate sciences (Kohonen, 2001; Liu and Weisberg, 2011; Landschützer et al., 2013, 2014). The use of SOM and other unsupervised machine learning approaches are becoming increasingly common in oceanography and have many possible applications in observational and model analysis (Liu and Weisberg, 2011; Liu et al., 2016; Jones et al., 2019; Rosso et al., 2020; Sonnewald et al., 2021; Boehme and Rosso, 2021). For example, Lu et al. (2019) use unsupervised clustering and a neural network to estimate subsurface temperature anomalies from surface data. We show that SOM analysis not only improves understanding of observed patterns but also can be leveraged to aid in the evaluation of a regional model.

To highlight the benefits of SOM in model evaluation, we train the SOM against ARGO and CTD temperature profiles. The SOM, an unsupervised neural network algorithm, is able to classify, or group, similar ocean temperature profiles together. The SOM analysis highlights observed spatio-temporal patterns within the upper ocean temperature. We then leverage the 'learned' vertical temperature structures (as determined by the SOM algorithm) in order to validate the TOPAZ ocean model. The SOM technique better retains small scale features seen in observations which are often lost due to spatial and temporal smoothing when validating model performance against gridded reanalysis or climatology products.

We show the TOPAZ ocean model captures the general spatial and temporal distribution of observed upper ocean characteristics, however, the SOM technique highlights several instances where the TOPAZ model contains critical deficiencies that would benefit from further improvement. In particular, the SOM technique captures instances where

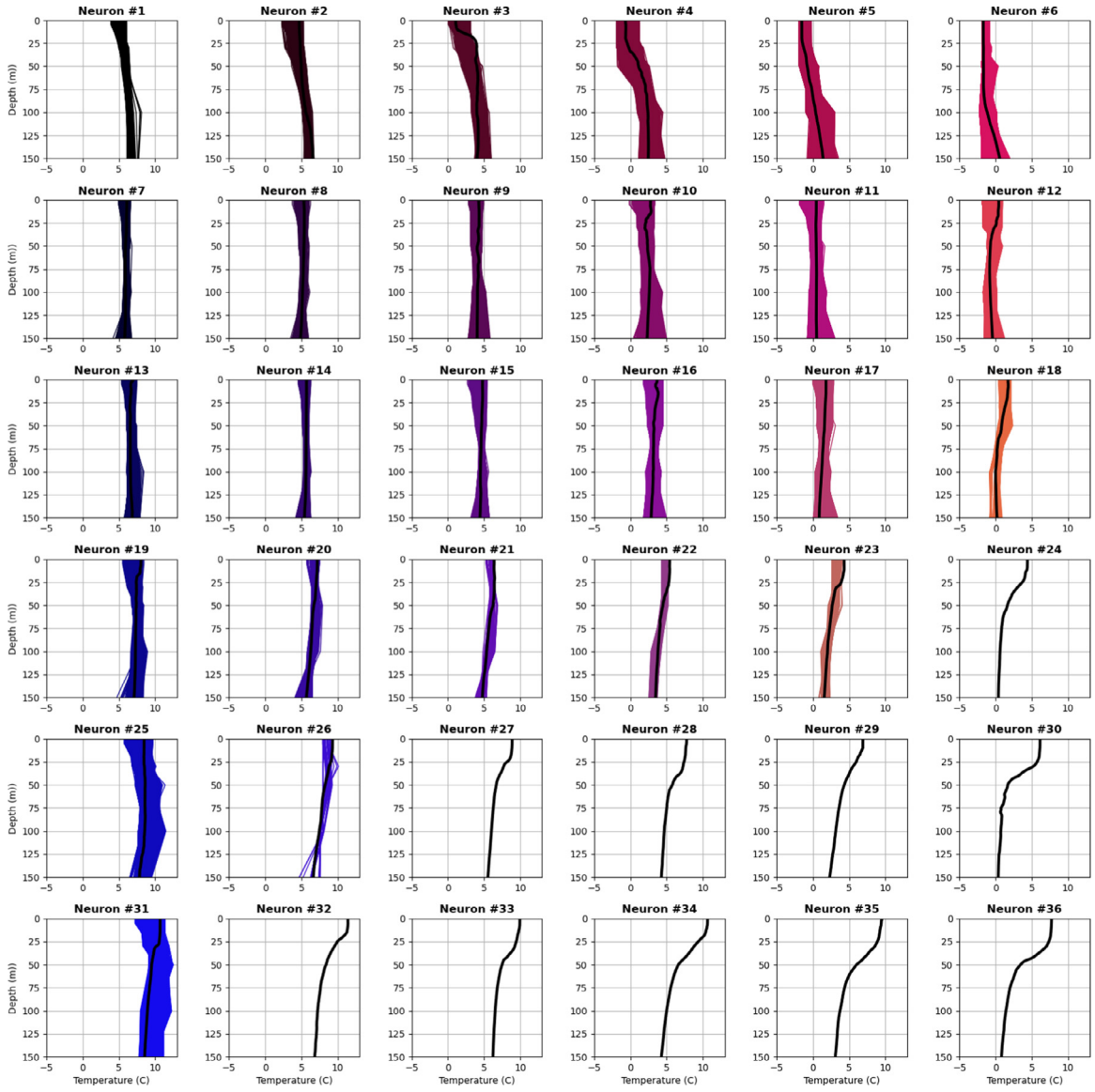


**Fig. 7.** Winter (DJF) TOPAZ temperature profiles (thin colored lines) sorted according to their best matching unit (BMU). The color of each observation represents the profile's best matching unit (BMU; numbered 1–36) as defined in Fig. 4. The BMU for each temperature profile is determined by the minimum Euclidean distance between the profile and each neuron weight. The neuron weights (shown with the thick black lines) are determined by the observation-based SOM as seen in Fig. 4.

the TOPAZ ocean model is unable to reproduce the spatial variability and upper ocean temperature features seen in observations.

Most notably, TOPAZ fails to capture the distinct separation of profile structures between the Greenland Basin and Lofoten Basin in all four seasons. Additionally, the SOM technique highlights how TOPAZ fails to simulate the observed upper ocean structures in the West Spitsbergen Current. Observations show the West Spitsbergen Current should be a tightly confined region with profiles closely representing the characteristics observed in the Lofoten Basin extending northward into the Arctic Ocean along the west and north sides of the Svalbard archipelago. TOPAZ, on the other hand, shows the West Spitsbergen Current contains characteristics of temperature profiles observed in the Greenland Basin, while the Lofoten basin-like temperature structures do not extend far enough north. Additionally, the current within TOPAZ appears overly diffuse, covering a larger region than observed on the west side of Svalbard. More generally, many structures simulated in TOPAZ, especially in JJA, contain too much thermal stratification and subsurface water temperatures below 50 m depth that are too cold.

Furthermore, TOPAZ struggles to capture the depth and temperature gradient of the observed thermocline, not only in the West Spitsbergen Current where TOPAZ performance is generally poor, but throughout the domain. This is especially true during summer months where warm SST is more prevalent. The poorly simulated thermocline structure within our domain appears to be intricately linked to the coarse vertical resolution archived from the TOPAZ model forecasts (the native vertical resolution of the TOPAZ model uses 28 hybrid layers but the TOPAZ output products are only archived at 12 vertical levels). This suggests there is a need not only for archiving more vertical levels from the TOPAZ ocean model to improve our understanding of the model deficiencies, but also for maintaining a minimum vertical resolution in the upper ocean within other ocean models used for Arctic forecasting purposes. This will become increasingly important as fully-coupled forecasting systems become more prevalent in the Arctic region.

Failing to simulate the observed upper ocean temperature characteristics in the Arctic could have serious implications on the accuracy of short term forecasts. Not capturing the observed thermocline structures suggests the model will likely also contain problems in simulating upper ocean mixing and surface heat fluxes. The SOM analysis showed the TOPAZ upper ocean stratification performs the worst in the boundary

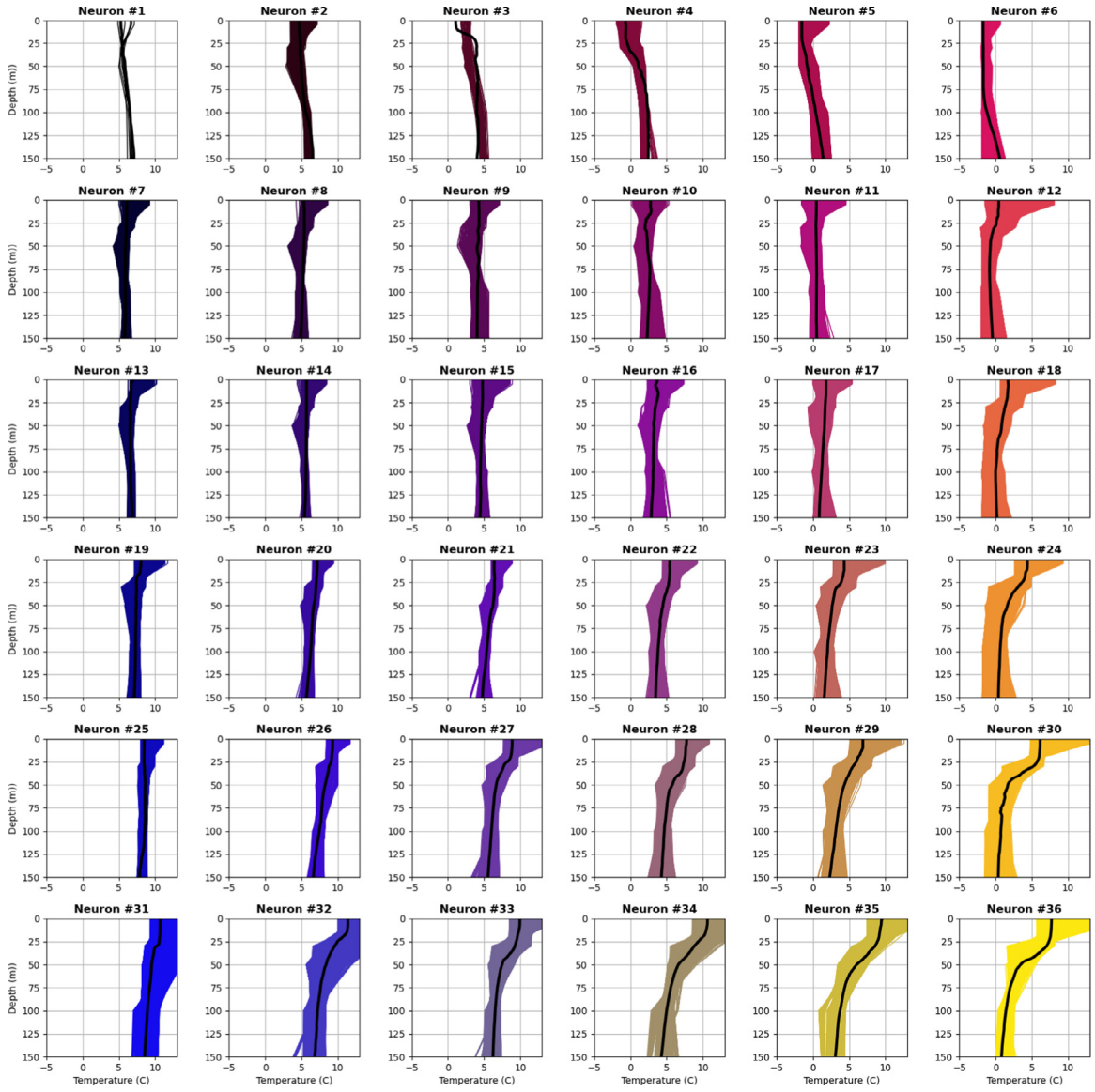


**Fig. 8.** Summer (JJA) TOPAZ temperature profiles (thin colored lines) sorted according to their best matching unit (BMU). The BMU for each TOPAZ temperature profile is determined by the minimum Euclidean distance between the profile and each neuron weight. The neuron weights (shown with the thick black lines) are determined by the observation-based SOM as seen in Fig. 4.

between the Greenland and Lofoten basins as well as in the West Spitsbergen Current. The incorrect upper ocean temperature structures and the spatially-diffuse nature of the simulated West Spitsbergen Current in TOPAZ could also impact the model's ability to simulate the correct sea ice behavior (such as melting and freeze rates) in this region. However, further analysis is needed to determine the exact relationship between the modeled TOPAZ upper-ocean temperatures and any direct impacts on the ocean mixing, surface heat fluxes or sea ice behavior.

We recognize that the TOPAZ ocean model forecasting product contains data assimilation of Argo and CTD temperature data, thus the TOPAZ forecast data used is not purely independent from the observations used to train the SOM in this analysis. However, we would like to mention the purpose of this study was not to perform a robust evaluation of the TOPAZ model against independent observations, but rather to highlight an underutilized, machine learning technique that has great potential in oceanography and earth sciences. In this study we highlight one potential application of SOM to the evaluation of gridded ocean products.

We initially tested the SOM technique using normalized temperature profiles. However, the observed separation (in SOM space) between the Greenland and Lofoten basin profiles is much less distinct when using normalized temperature profiles. In other words, the SOM is unable to clearly categorize profiles in our region when using normalized temperature profiles. Non-normalized temperature profiles provide clean spatial and temporal separation between various oceanographic features thus allowing the best assessment of model performance. However, we expect many applications of self-organizing maps in earth sciences and oceanography would benefit more from the use of normalized data.

One future effort utilizing normalized data will be to expand this analysis to multivariate data, such as integrating salinity into the SOM analysis. Although salinity profiles are neglected in the present study, they will be included in future efforts in order to analyze the density structure and vertical stability of this region similar to the Gaussian mixture modeling technique used by Thomas et al. (2021a). A multivariate approach may also help classify oceanographic features identifiable through salinity or density characteristics as opposed to temperature characteristics alone.

One benefit of SOM and other common unsupervised clustering techniques, such as K-means clustering, over supervised machine learning techniques is requiring no user input during the training process.

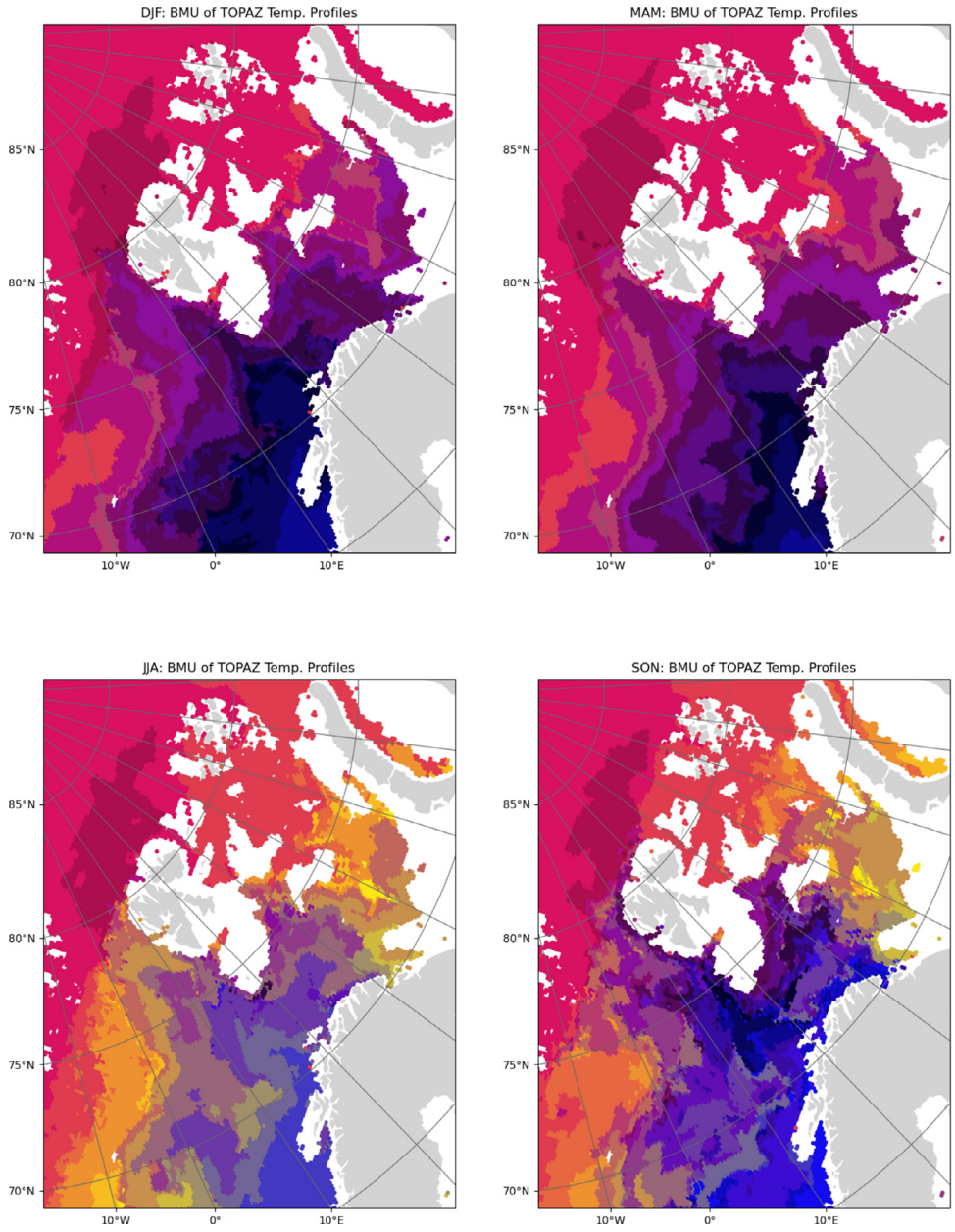


**Fig. 9.** Spatial distribution of TOPAZ temperature profiles for each season: DJF, MAM, JJA, SON. The colors represent the best matching unit (BMU) as defined in Fig. 4. White spaces indicate locations where the TOPAZ ocean depth is less than 200 m which are ignored in our analysis. Since we use daily temperature data in out analysis, the BMU plotted at any given spatial location shows the mode of all daily BMU values in the three month period (in other words, this figure shows the BMU that occurs most often during the three month period).

This allows the model itself to identify and isolate characteristics and patterns within complex non-linear data sets. One difference between SOM and K-means clustering is the self-organizing nature of the neurons in SOM. K-means clustering contains exclusive partitioning (where each piece of data can only belong to one neuron or cluster) within a pre-defined number of clusters. While SOM also contains exclusive partitioning, the SOM training process allows the structure of each neuron to influence the structures of the neighboring neurons. Therefore, neighboring neurons in the SOM share common features which helps when identifying large-scale spatial and temporal patterns and shared characteristics within the data, without requiring the data to exist within the exact same cluster or neuron. This self-organization of the clusters and shared features between neighboring neurons made SOM an appropriate choice for our purpose of quickly identifying spatial and temporal patterns in observations and model data containing large variability, such as upper ocean temperatures in the Arctic.

One significant caveat of SOM, and machine learning techniques in general, is the inability of the algorithm to 'learn' when large gaps in the training data exist. The types of temperature structures identified by SOM (the neuron weights) are limited by the available observations used to train the neural network. For example, the eastern Barents Sea region is under sampled in every season. If unique temperature structures exist in this poorly sampled region and are not represented in the training data set, SOM is unable to identify and categorize these types of profile structures. Like all model evaluation techniques, model evaluation with SOM is particularly challenging and results in larger uncertainties in regions with poor observational coverage. Another limitation of SOM is the sensitivity to the number of neurons used. Using too many neurons does not generate useful, distinct clusters and provides little useful information about characteristics within the data. On the other hand, too few neurons results in a poor fit between the data and its assigned neuron weight. This is due to overly large volumes

**Table 1**
Seasonal mean Q-errors (in K) comparing temperature observations and TOPAZ data to the SOM neuron weights.

| | DJF | MAM | JJA | SON |
|---|---|---|---|---|
| Obs | 4.17 | 4.20 | 6.79 | 6.92 |
| TOPAZ | 5.07 | 4.99 | 7.57 | 7.23 |

of data assigned to any given neuron which smooths distinctive structures of the neuron weights. It is worth noting that K-means clustering also suffers from this limitation.

Unsupervised machine learning techniques, like self-organizing maps, have great potential in future oceanography and earth science research. SOM can provide additional, beneficial knowledge when used in combination with other evaluation techniques of modeled subsurface ocean temperature. The SOM technique presented here is able to classify upper ocean temperature characteristics while retaining some of the observed small-scale variability that is typically lost when validating models against reanalysis data sets which highlights instances where ocean models under-represent observations. In order to continue improving model representation of upper ocean temperature variability and the accuracy of coupled forecasting systems, the results shown here indicate continued need for ocean model development, advances in data assimilation of ocean observations into ocean models, and increased observational coverage in the Arctic.

## CRediT authorship contribution statement

**Erin E. Thomas:** Conceptualization, Methodology, Investigation, Formal analysis, Visualization, Writing – original draft. **Malte Müller:** Formal analysis, Visualization, Writing – review & editing.

## Declaration of competing interest

The authors declare that they have no known competing financial interests or personal relationships that could have appeared to influence the work reported in this paper.

## Data availability

All Argo, CTD observations as well as the TOPAZ model forecast data used in this study are accessible through the Copernicus Marine Environmental Monitoring service. The TOPAZ output products are available here: https://doi.org/10.48670/moi-00001 and in-situ observations (ARGO and CTD) are available here: https://doi.org/10.48670/moi-00036.

## Acknowledgments

Financial support for this work was provided by the Norwegian Research Council under the Nansen Legacy (NFR-276730) and FOCUS (NFR-301450) projects.

## Appendix A. Supplementary data

Supplementary material related to this article can be found online at https://doi.org/10.1016/j.ocemod.2022.102092.

## References

Aagaard, K., Swift, J.H., Carmack, E.C., 1985. Thermohaline circulation in the Arctic Mediterranean Seas. J.L Geophys. Res. 90 (C3), 4833–4846. http://dx.doi.org/10.1029/JC090iC03p04833.

Batrak, Y., Müller, M., 2018. Atmospheric response to kilometer-scale changes in sea ice concentration within the marginal ice zone. Geophys. Res. Lett. 45 (13), 6702–6709. http://dx.doi.org/10.1029/2018GL078295.

Batrak, Y., Müller, M., 2019. On the warm bias in atmospheric reanalyses induced by the missing snow over arctic sea-ice. Nat. Comm. 10 (1), 4170. http://dx.doi.org/10.1038/s41467-019-11975-3.

Bauer, P., Beljaars, A., Ahlgrimm, M., Bechtold, P., Bidlot, J.-R., Bonavita, M., Bozzo, A., Forbes, R., Hólm, E.V., Leutbecher, M., Lopez, P., Magnusson, L., Prates, F., Rodwell, M., Sandu, I., Untch, A., Vitart, F., 2013. Model cycle 38r2: Components and performance. (704), p. 58. http://dx.doi.org/10.21957/xc1r0lj6l, URL https://www.ecmwf.int/node/7986.

Boehme, L., Rosso, I., 2021. Classifying oceanographic structures in the Amundsen sea, Antarctica. Geophys. Res. Lett. 48 (5), http://dx.doi.org/10.1029/2020GL089412.

Canuto, V.M., Howard, A., Cheng, Y., Dubovikov, M.S., 2002. Ocean turbulence. Part II: Vertical diffusivities of momentum, heat, salt, mass, and passive scalars. J. Phys. Oceanogr. 32, 240–264. http://dx.doi.org/10.1175/1520-0485(2002)032<0240:OTPIVD>2.0.CO;2.

Cronin, M.F., Gentemann, C.L., Edson, J., Ueki, I., Bourassa, M., Brown, S., Clayson, C.A., Fairall, C.W., Farrar, J.T., Gille, S.T., Gulev, S., Josey, S.A., Kato, S., Katsumata, M., Kent, E., Krug, M., Minnett, P.J., Parfitt, R., Pinker, R.T., Stackhouse, P.W., Swart, S., Tomita, H., Vandemark, D., Weller, A.R., Yoneyama, K., Yu, L., Zhang, D., 2019. Air-sea fluxes with a focus on heat and momentum. Front. Mar. Sci. 6, URL https://www.frontiersin.org/article/10.3389/fmars.2019.00430.

D'Asaro, E.A., 2014. Turbulence in the upper-ocean mixed layer. Ann. Rev. Mar. Sci. 6 (1), 101–115. http://dx.doi.org/10.1146/annurev-marine-010213-135138, PMID: 23909456.

Giorgi, F., 2019. Thirty years of regional climate modeling: Where are we and where are we going next? J. Geophys. Res. 124 (11), 5696–5723. http://dx.doi.org/10.1029/2018JD030094.

Hall, C.M., Saarinen, J., 2010. Polar tourism: Definitions and dimensions. Scandinavian J. Hospitality Tourism 10, 448–467. http://dx.doi.org/10.1080/15022250.2010.521686.

Helland-Hansen, B., Nansen, F., 1909. The Norwegian Sea: its physical oceanography based upon the Norwegian Research 1900–1904. Technical Report 2, Report on Norwegian Fishery and Marine Investigations.

Hunke, E.C., Dukowicz, J.K., 1997. An elastic–Viscous–plastic model for sea ice dynamics. J. of Phys. Oceanogr. 27 (9), 1849–1867. http://dx.doi.org/10.1175/1520-0485(1997)027<1849:AEVPMF>2.0.CO;2.

Iskandar, I., Tozuka, T., Masumoto, Y., Yamagata, T., 2008. Impact of Indian Ocean Dipole on intraseasonal zonal currents at 90% E on the equator as revealed by self-organizing map. Geophys. Res. Lett. 35 (14), http://dx.doi.org/10.1029/2008GL033468.

Jones, D.C., Holt, H.J., Meijers, A.J.S., Shuckburgh, E., 2019. Unsupervised clustering of Southern Ocean Argo Float temperature profiles. J. Geophys. Res. 124 (1), 390–402. http://dx.doi.org/10.1029/2018JC014629.

Kohonen, T., 2001. Self-Organizing Maps, 3rd Springer, Berlin.

Landschützer, P., Gruber, N., Bakker, D.C.E., Schuster, U., 2014. Recent variability of the global ocean carbon sink. Glob. Biogeochem. Cycles 28 (9), 927–949. http://dx.doi.org/10.1002/2014GB004853.

Landschützer, P., Gruber, N., Bakker, D.C.E., Schuster, U., Nakaoka, S., Payne, M.R., Sasse, T.P., Zeng, J., 2013. A neural network-based estimate of the seasonal to inter-annual variability of the Atlantic Ocean carbon sink. Biogeosciences 10 (11), 7793–7815. http://dx.doi.org/10.5194/bg-10-7793-2013.

Liu, Y., Weisberg, R.H., 2011. A review of self-organizing map applications in meteorology and oceanography. In: Mwasiagi, J.I. (Ed.), Self Organizing Maps. Intech, Rijeka, Croatia, http://dx.doi.org/10.5772/13146.

Liu, Y., Weisberg, R.H., Vignudelli, S., Mitchum, G.T., 2016. Patterns of the loop current system and regions of sea surface height variability in the eastern Gulf of Mexico revealed by the self-organizing maps. J. Geophys. Res. 121 (4), 2347–2366. http://dx.doi.org/10.1002/2015JC011493.

Lu, W., Su, H., Yang, X., Yan, X.-H., 2019. Subsurface temperature estimation from remote sensing data using a clustering-neural network method. Remote Sens. Environ. 229, 213–222. http://dx.doi.org/10.1016/j.rse.2019.04.009.

Melsom, A., Counillon, F., LaCasce, J., Bertino, L., 2012. Forecasting search areas using ensemble ocean circulation modeling. Ocean Dyn. 62, 1245–1257. http://dx.doi.org/10.1007/s10236-012-0561-5.

Mork, K.A., Skagseth, Ø., 2010. A quantitative description of the Norwegian Atlantic Current by combining altimetry and hydrography. Ocean Sci. 6 (4), 901–911. http://dx.doi.org/10.5194/os-6-901-2010.

Müller, M., Batrak, Y., Kristiansen, J., Køltzow, M.A.Ø., Noer, G., Korosov, A., 2017. Characteristics of a convective-scale weather forecasting system for the European Arctic. Mon. Wea. Rev. 145 (12), 4771–4787. http://dx.doi.org/10.1175/MWR-D-17-0194.1.

Raj, R., Chatterjee, S., Bertino, L., Turiel, A., Portabella, M., 2019. The arctic front and its variability in the Norwegian Sea. Ocean Sci. 15, 1729–1744. http://dx.doi.org/10.5194/os-15-1729-2019.

Richardson, A., Risien, C., Shillington, F., 2003. Using self-organizing maps to identify patterns in satellite imagery. Progr. Oceanogr. 59 (2), 223–239. http://dx.doi.org/10.1016/j.pocean.2003.07.006.

Rossby, T., 1996. The North Atlantic current and surrounding waters: At the crossroads. Rev. Geophys. 34, 463–481.

Rosso, I., Mazloff, M.R., Talley, L.D., Purkey, S.G., Freeman, N.M., Maze, G., 2020. Water mass and biogeochemical variability in the kerguelen sector of the southern ocean: A machine learning approach for a mixing hot spot. J. Geophys. Res. Oceans 125 (3), http://dx.doi.org/10.1029/2019JC015877.

Sakov, P., Counillon, F., Bertino, L., Lisæter, K.A., Oke, P.R., Korablev, A., 2012. TOPAZ4: an ocean-sea ice data assimilation system for the North Atlantic and Arctic. Ocean Sci. 8 (4), 633–656. http://dx.doi.org/10.5194/os-8-633-2012.

Skagseth, Ø., Orvik, K.A., Furevik, T., 2004. Coherent variability of the norwegian atlantic slope current derived from TOPEX/ERS altimeter data. Geophys. Res. Lett. 31 (14), http://dx.doi.org/10.1029/2004GL020057.

Smith, L.C., Stephenson, S.R., 2013. New trans-arctic shipping routes navigable by midcentury. Proc. Natl. Acad. Sci. USA 110, http://dx.doi.org/10.1073/pnas.1214212110.

Sonnewald, M., Lguensat, R., Jones, D.C., Dueben, P.D., Brajard, J., Balaji, V., 2021. Bridging observations, theory and numerical simulation of the ocean using machine learning. Environ. Res. Lett. 16 (7), 073008. http://dx.doi.org/10.1088/1748-9326/ac0eb0.

Stocker, A.N., Renner, A.H., Knol-Kauffman, M., 2020. Sea ice variability and maritime activity around svalbard in the period 2012–2019. Sci. Rep. 10, http://dx.doi.org/10.1038/s41598-020-74064-2.

Swift, J.H., Aagaard, K., 1981. Seasonal transitions and water mass formation in the iceland and greenland seas. Deep Sea Res. Part A 28 (10), 1107–1129. http://dx.doi.org/10.1016/0198-0149(81)90050-9.

Thomas, S.D.A., Jones, D.C., Faul, A., Mackie, E., Pauthenet, E., 2021a. Defining Southern Ocean fronts using unsupervised classification. Ocean Sci. 17 (6), 1545–1562. http://dx.doi.org/10.5194/os-17-1545-2021.

Thomas, E.E., Müller, M., Bohlinger, P., Batrak, Y., Szapiro, N., 2021b. A kilometer-scale coupled atmosphere-wave forecasting system for the European Arctic. Wea. Forecasting 36 (6), 2087–2099. http://dx.doi.org/10.1175/WAF-D-21-0065.1.

Wehde, H., Schuckmann, K.V., Pouliquen, S., Grouazel, A., Bartolome, T., Tintore, J., AlonsoMunoyerro, M.A., Carval, T., Racapé, V., 2021. Quality Information Document - for Neat Real Time IN SITU products. Technical Report, Copernicus Marine Environmental Monitoring Service, URL https://resources.marine.copernicus.eu/product-detail/INSITU_ARC_NRT_OBSERVATIONS_013_031/DOCUMENTATION.

Wong, A.P.S., Wijffels, S.E., Riser, S.C., Pouliquen, S., Hosoda, S., Roemmich, D., Gilson, J., Johnson, G.C., Martini, K., Murphy, D.J., Scanderbeg, M., Bhaskar, T.V.S.U., Buck, J.J.H., Merceur, F., Carval, T., Maze, G., Cabanes, C., André, X., Poffa, N., Yashayaev, I., Barker, P.M., Guinehut, S., Belbéoch, M., Ignaszewski, M., Baringer, M.O., Schmid, C., Lyman, J.M., McTaggart, K.E., Purkey, S.G., Zilberman, N., Alkire, M.B., Swift, D., Owens, W.B., Jayne, S.R., Hersh, C., Robbins, P., WestMack, D., Bahr, F., Yoshida, S., Sutton, P.J.H., Cancout, R., Coatanoan, C., Dobbler, D., Juan, A.G., Gourrion, J., Kolodziejczyk, N., Bernard, V., Bourlès, B., Claustre, H., D'Ortenzio, F., Le Reste, S., Le Traon, P.-Y., Rannou, J.-P., SaoutGrit, C., Speich, S., Thierry, V., Verbrugge, N., Angel-Benavides, I.M., Klein, B., Notarstefano, G., Poulain, P.-M., VélezBelchí, P., Suga, T., Ando, K., Iwasaska, N., Kobayashi, T., Masuda, S., Oka, E., Sato, K., Nakamura, T., Sato, K., Takatsuki, Y., Yoshida, T., Cowley, R., Lovell, J.L., Oke, P.R., van Wijk, E.M., Carse, F., Donnelly, M., Gould, W.J., Gowers, K., King, B.A., Loch, S.G., Mowat, M., Turton, J., Rama Rao, E.P., Ravichandran, M., Freeland, H.J., Gaboury, I., Gilbert, D., Greenan, B.J.W., Ouellet, M., Ross, T., Tran, A., Dong, M., Liu, Z., Xu, J., Kang, K., Jo, H., Kim, S.-D., Park, H.-M., 2020. Argo data 1999–2019: Two million temperature-salinity profiles and subsurface velocity observations from a global array of profiling floats. Front. Mar. Sci. 7, http://dx.doi.org/10.3389/fmars.2020.00700.